energies

MDPI

Article

Study on Windage Response Suppression of Large-Span Transmission Tower-Line System Using a Spring-Pendulum Dynamic Vibration Absorber

Peng Song [1], Xujun Lang [1], Sixiang Zhang [1], Bo Yang [1], Siyao Zhang [2], Kunjie Rong [2,*] and Li Tian [2]

[1] Shandong Electric Power Engineering Consulting Institute Co., Ltd., Jinan 250013, China
[2] School of Civil Engineering, Shandong University, Jinan 250061, China
* Correspondence: kunjierong@sdu.edu.cn; Tel.: +86-15965638070

Abstract: Insulators and conductors in transmission line systems are susceptible to wind-induced movements, especially when insulators are closely positioned to transmission towers, potentially leading to electrical discharge. To address this issue, this study proposes a spring-pendulum dynamic vibration absorber (SPDVA) for windage suppression in transmission line systems. Using a finite element model based on an actual transmission line project, the study investigates SPDVA's effectiveness in mitigating windage responses under varying wind speeds. The analysis considers mass and stiffness parameters to elucidate SPDVA's suppression mechanism. The results indicate that SPDVA outperforms the additional heavy hammer method in suppressing insulator windage responses and also affects the peak acceleration response at the insulator's bottom. Increasing stiffness initially enhances SPDVA's suppression effectiveness on both peak and mean square deviation windage angle responses, peaking at 10 kN/m stiffness, while increasing the mass of the mass block also enhances suppression effectiveness.

Keywords: large-span transmission tower-line system; windage response; heavy hammer; spring-pendulum dynamic vibration absorber; windage suppression mechanism

Citation: Song, P.; Lang, X.; Zhang, S.; Yang, B.; Zhang, S.; Rong, K.; Tian, L. Study on Windage Response Suppression of Large-Span Transmission Tower-Line System Using a Spring-Pendulum Dynamic Vibration Absorber. *Energies* **2024**, *17*, 5638. https://doi.org/10.3390/en17225638

Academic Editor: Giovanni Lutzemberger

Received: 11 October 2024
Revised: 29 October 2024
Accepted: 7 November 2024
Published: 11 November 2024

1. Introduction

The rapid economic and social development in China presents challenges to the efficient operation of power grid systems, particularly with the expansion of large-span and ultra-high voltage (UHV) transmission line systems (1000 kV and above alternating current grid or ±800 kV and above direct current grid). These structures are more susceptible to wind-induced problems such as insulator and conductor sway under strong wind loads. Close proximity between insulators and transmission towers can lead to discharge, while wide conductor spacing necessitates broader corridor widths for transmission lines. Consequently, there is an urgent need for research into the wind-induced responses of transmission lines and the development of effective windage suppression measures.

Various scholars have studied the dynamic behavior of conductors and insulators under wind loads [1–10]. Many have employed finite element simulations to analyze windage in greater detail. For instance, Dominik et al. [11] proposed a model for predicting wind-induced oscillations in new overhead transmission lines, while Haddadin et al. [12] analyzed line and tower responses under different wind speeds using spectrum analysis. Scholars like Wang et al. [13] applied the random vibration theory to model wire deflection responses, comparing nonlinear and linear methods. Others focused on the aerodynamic properties of conductors, considering dynamic wind effects and aerodynamic damping [14,15]. Fu et al. [16] explored wind–rain interactions affecting overhead lines during typhoons.

Structural vibration control technology is an effective way to suppress structural excessive response [17,18]; addressing windage challenges, researchers have proposed

various suppression measures. Xu et al. [19] used a finite element model to assess windage suppression methods for composite insulators, highlighting effective strategies like V-type strings and guyed wires. Rao et al. [20] investigated conductor windage accidents, proposing mitigation measures based on field data. Chen et al. [21] calculated wind deflection angles for suspension insulators before and after installing heavy hammers, showing favorable reductions. Zheng et al. [22] reported load increases and windage angle decreases after heavy hammer installations in practical projects. Lu et al. [23] modeled V-type composite insulators using the ABAQUS 2017 software, analyzing their deformation and windage characteristics. Tian et al. [24] adopted a tuned mass damper to control the wind-induced responses of a transmission tower-line system.

Despite these efforts, the existing windage suppression methods such as heavy hammers and composite insulator strings have limitations in terms of application scope and effectiveness. Moreover, research attention on insulator's vibration responses under wind load remains sparse. Consequently, this study proposes a novel spring-pendulum dynamic vibration absorber (SPDVA) for suppressing windage responses in transmission line systems. Compared to traditional methods, SPDVA utilizes chaotic spring-pendulum motion to enhance vibration energy absorption and dissipation, thereby improving suppression efficiency.

This study conducts the wind-induced response analyses of transmission line systems to determine critical wind speeds for windage, and a spring-pendulum dynamic vibration absorber (SPDVA) is proposed to suppress the windage response of transmission line systems. In Section 2, based on the 1000 kV transmission line project, the finite element model of a large-span transmission tower-line system is established, and the windage response of the transmission tower-line system and the suppression effectiveness of the SPDVA are analyzed and discussed. Section 3 carried out a parametric analysis, and the suppression law considering mass and stiffness parameters is investigated, and Section 4 is the conclusion. The research results can provide a reference for the windage suppression method of actual transmission line systems.

2. Windage Response Analysis of Transmission Tower-Line System

2.1. Finite Element Model

A 1000 kV transmission line project in Jiangxi Province of China is selected as the research object, with a total span of 2860 m, including one tangent tower and two span transmission lines. The tangent tower is made of Q420 and Q345 steel pipes with a total height of 169 m, the span of transmission lines is 1430 m, and each span of the transmission line is divided into four layers [25]. The upper layer is the ground wire and the lower three layers are the wires, and the sag is determined by the local average temperature. Figure 1 shows the plane design of the transmission tower. Details of the conductor and ground wire are shown in Table 1.

Table 1. Comparison of numerical simulation and measured data.

Type	Conductor	Ground Wire
Name	JLHA1/G4A-500/230	OPGW-300
Source of equipment	AnHui Electric Group Shares Co., Ltd., Chuzhou, China	AnHui Electric Group Shares Co., Ltd., Chuzhou, China
Elastic modulus (GPa)	97.0	170.1
Sectional area (mm^2)	727.93	295.4
Outside diameter (mm)	35.13	22.90
Calculated weight (kg/km)	3173.5	2166.0
Expansion coefficient (1/°C)	16.0×10^{-6}	13.0×10^{-6}

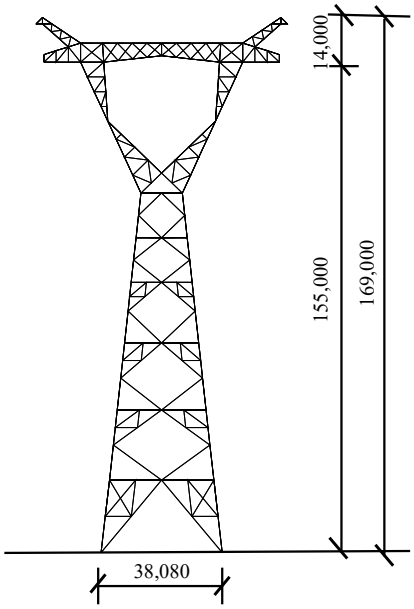

Figure 1. Design plan of the tangent tower (unit: mm).

The finite element model of the transmission tower-line system is established in ABAQUS. The vertical tower-line direction is defined as X, the direction along the tower line is defined as Y, and the vertical direction is defined as Z, as shown in Figure 2. The elastic modulus of the steel is 2.06 $\times$ 10^5 MPa, the mass density is 7850 kg/m^3, and the Poisson's ratio is 0.3. The members are simulated by the B31 beam element, and the insulators and transmission lines are simulated by the T3D2 element. The bilinear strengthening model is used to simulate the mechanical behavior of the materials. The rigid constraint is set at the tower leg, and the hinge constraint is set at both ends of the transmission line. Through form-finding, the transmission lines reach the predetermined sags under the action of gravity, while the insulators are kept in a vertical position.

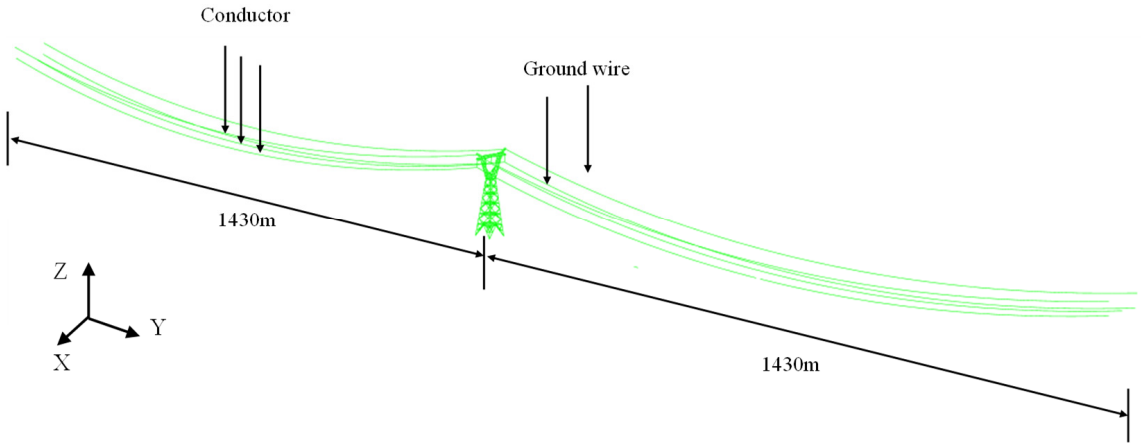

Figure 2. Finite element model of transmission tower-line system.

2.2. Wind Load Simulation

The wind speed at any point in nature can be regarded as the superposition of long-period mean wind and short-period fluctuating wind, which is expressed by the following formula:

$$v(z,t) = \overline{v}(z) + v_f(z,t) \quad (1)$$

where $\overline{v}(z)$ is the average wind speed, and $\overline{v}_f(z,t)$ is the fluctuating wind speed.

The exponential wind profile is used to describe the variation in average wind speed along the boundary layer height. The expression is as follows:

$$\overline{v}(z) = V_{10}\left(\frac{z}{10}\right)^{\alpha} \tag{2}$$

where z is the height of any point, V_{10} is the wind speed at the height of 10 m, and α is the turbulence; this paper takes an amount of 0.15 [26].

The time history of fluctuating wind speed is regarded as a stationary Gaussian random process, which is simulated by the linear filtering method in this study. Considering that the total height of the transmission tower-line system is large, the Kaimal spectrum [27] of the horizontal fluctuating wind speed spectrum with height variation is used in the calculation. The expression is as follows:

$$\frac{nS_v(n)}{u_*^2} = \frac{200x}{(1+50)^{5/3}} \tag{3}$$

where $S(n)$ is the self-spectral density function of the fluctuating wind speed process; x is a function positively correlated with the frequency and height of fluctuating wind; u_* is the friction velocity; and n is the frequency of fluctuating wind.

According to the structural characteristics of the transmission tower, based on the International Electrotechnical Commission IEC (60826-2003) [28] specification, the following formula is used to calculate the wind load acting on the transmission tower:

$$F(t) = \frac{1}{2}\rho_a V^2(t)(1+0.2sin^2 2\theta)(A_1 C_{xt1}\cos^2\theta + A_2 C_{xt2} sin^2\theta)G_t \tag{4}$$

$$F_x(t) = F(t)cos\theta \tag{5}$$

$$F_y(t) = F(t)sin\theta \tag{6}$$

where F_x and F_y are the components of the wind load acting on the transmission tower in the X and Y horizontal directions, respectively; θ is the wind attack angle, which is defined as the angle between the wind direction and the X direction; ρ_a is the air density, take 1.225 kg/m^3; V is the wind speed at the height of 10 m; A_1 and A_2 are the lateral and longitudinal wind-shielding area of the transmission tower, respectively; C_{xt1} and C_{xt2} are the lateral and longitudinal resistance coefficients perpendicular to the tower body; and G_t is the wind load combination coefficient of the structure.

The wind load acting on the transmission line is as follows:

$$F_c(t) = q_0 C_{xc} C_c C_L dL sin^2\Omega \tag{7}$$

where q_0 is the basic wind pressure; C_{xc} is the resistance coefficient of the transmission line, usually take 1.00; C_c is the wind load combination coefficient of the transmission line depending on the height and terrain category; C_L is the span coefficient of the transmission line; d is the diameter of the transmission line; L is the horizontal span of the transmission line; and Ω is the angle between the wind direction and the transmission line.

When simulating the wind load acting on the transmission tower, the transmission tower is divided into eight sections from bottom to top, and the wind-shielding area of each section of the tower is calculated, respectively. The wind speed at the midpoint of each internode is taken as the wind speed in the corresponding simulation area, as shown in Figure 3. The length of the wire element is 10 m, and the wind load is applied at the node.

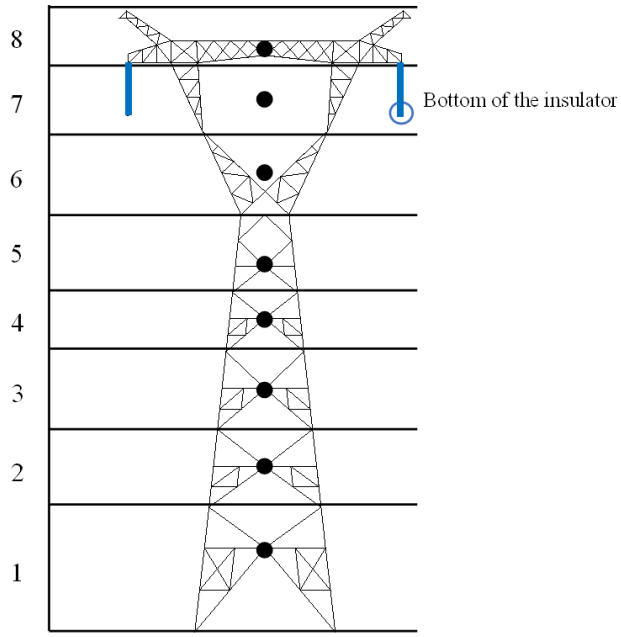

Figure 3. Sectional schematic diagram of wind load simulation.

The wind speed at the height of 10 m is 30 m/s, and the wind load simulation time interval is 0.1 s. The 120 s wind load time history of the tower-line system is generated. Figure 4 shows the comparison of the wind speed time history and simulation results at the bottom of the insulator. It can be concluded that the wind load simulation spectrum is consistent with the target spectrum trend, and the overall fitting is good, which proves that the simulation results are reliable and can be used for the subsequent analysis.

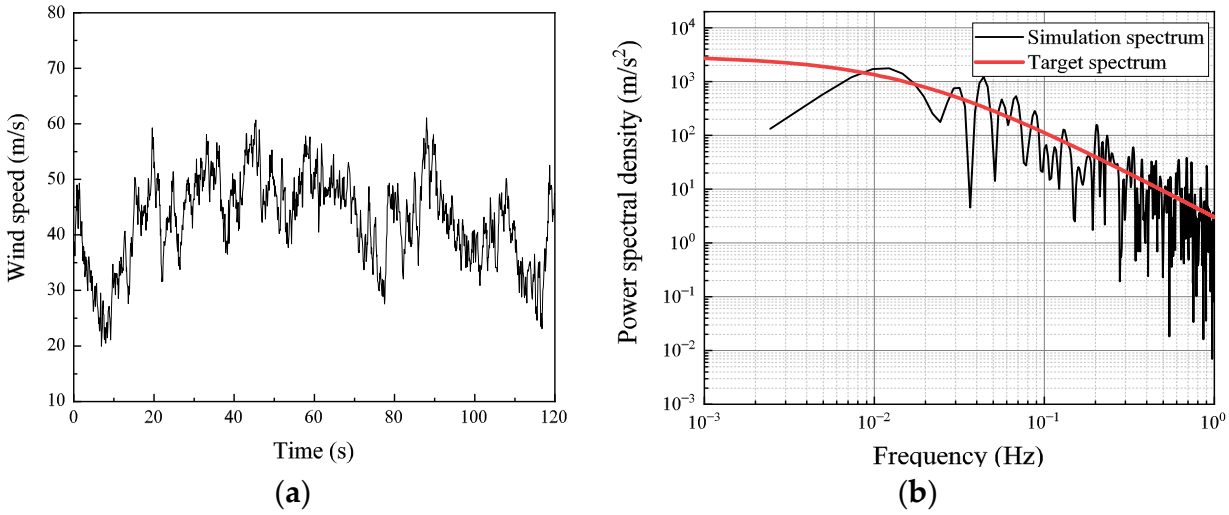

Figure 4. (**a**) Wind speed time series; (**b**) comparison of simulation results.

2.3. Analysis of Windage Response

To analyze how wind speed affects the peak windage angle of the insulator, a finite element simulation is conducted in ABAQUS using generated fluctuating wind loads. Figure 5 illustrates the impact of wind speed at a 10 m height on the insulator's peak windage angle. The results show that the peak windage angle increases linearly with the wind speed. According to the relative position of the bottom of the insulator and the transmission tower, the windage shape of the insulator is calculated, and the windage angle of the insulator is obtained ($\alpha = sin^{-1}((l_0 - l_1)/l)$; among them, α is the angular measure-

ment, l_0 is the distance from the component to the vertical position of the insulator, l_1 is the minimum allowable gap between the double-circuit charged part and the component, and l is the length of the insulator). According to relevant specifications [25], the minimum allowable gap between the double-circuit charged part and the tower component under power frequency voltage is 2.7 m, corresponding to a maximum allowable windage angle of 58.39°. The figure indicates that at a wind speed of 26 m/s, the peak windage angle exceeds this maximum allowable value, identifying 26 m/s as the critical wind speed.

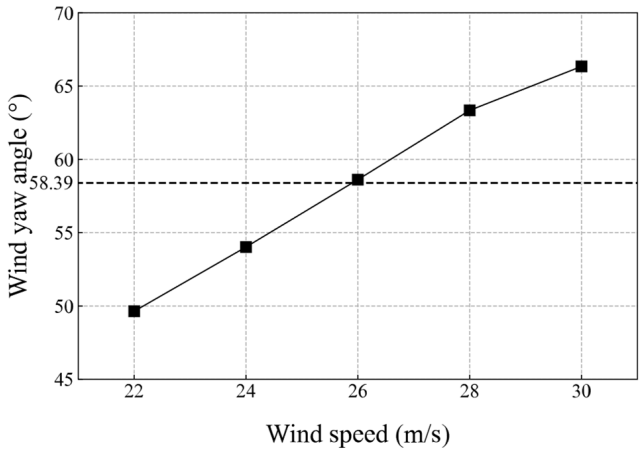

Figure 5. The influence of wind speed change on the windage angle.

3. Windage Response Suppression Analysis

3.1. Spring-Pendulum Dynamic Vibration Absorber

Based on the results of the windage response analysis of transmission line systems, it is necessary to propose effective windage suppression measures to reduce the windage response. At present, the windage suppression method of insulators is generally to install a heavy hammer at the bottom [21,22], and the additional gravity is used to balance the horizontal force of the wind load. However, the application of this method requires a large hammer mass, and the windage suppression effectiveness is limited. Therefore, a spring-pendulum dynamic vibration absorber is proposed based on the principle of a spring-pendulum. The insulator vibrates under wind load and the SPDVA goes into a working state, transferring the vibration energy to the mass block system and dissipating it with the help of a viscous damping element. The spring-pendulum mechanism allows the device to couple with the multiple vibration modes of the insulator to form irregular motions, thus enhancing the vibration absorption effect. Figure 6 shows the simulation diagram of the SPDVA in ABAQUS. The SPDVA is installed at the lower part of the insulator; among them, the mass block is established by a MASS element, and the mass block is connected to the insulator by a SPRING element.

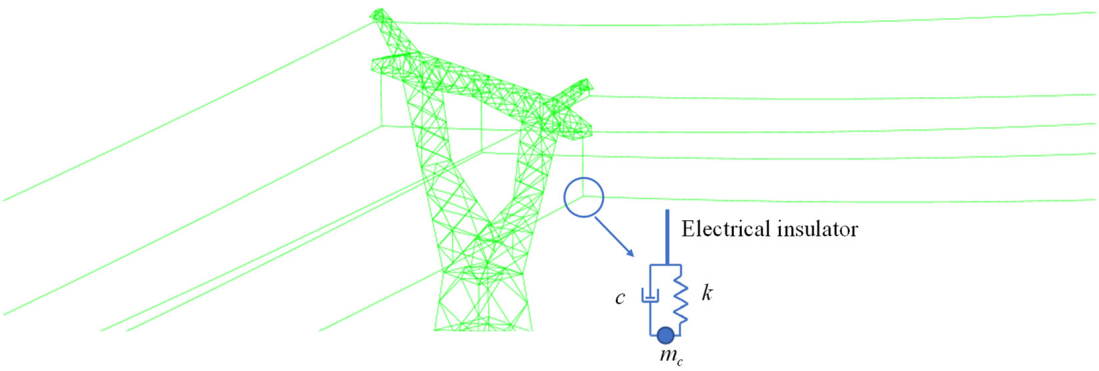

Figure 6. Numerical modeling approach of SPDVA.

Table 2 shows the configuration parameters of the SPDVA suitable for the transmission tower-line system. In order to highlight the windage suppression effect of the SPDVA, the traditional suppression scheme with a heavy hammer is also designed. The weight of the heavy hammer is consistent with the mass of the mass block in the SPDVA, which is 6000 kg and installed at the insulator's bottom.

Table 2. Design parameters of SPDVA.

Design Parameter	m_c (kg)	k (kN/m)	c (kN/(m/s))	l_0 (m)
Value	6000	10	10	1

To quantify the suppression effectiveness of the SPDVA on the insulator's windage response, the peak and mean square deviation suppression ratios (η and γ) of the device are defined as follows:

$$\eta = \frac{P_n - P_d}{P_n} \times 100\% \tag{8}$$

$$\gamma = \frac{R_n - R_d}{R_n} \times 100\% \tag{9}$$

where P_d and P_n represent the peak values of windage response with SPDVA control and without control, respectively, and R_d and R_d represent the mean square deviation values of windage response with SPDVA control and without control, respectively.

3.2. Windage Suppression Effectiveness

The critical wind speed is 26 m/s at the height of 10 m, and three working conditions of without control, heavy hammer control, and SPDVA control are set up to analyze the effectiveness of the SPDVA on the transmission tower-line system. Figure 7 shows the response time history curve of the insulator's windage angle. The peak windage angles under the heavy hammer and SPDVA control are significantly lower than in the uncontrolled state. Specifically, the peak windage angle is 58.62° in the uncontrolled state, 51.61° with the heavy hammer (an 11.96% reduction), and 49.32° with the SPDVA (a 15.86% reduction). Therefore, the SPDVA provides a more effective suppression of the insulator's windage angle compared to the heavy hammer.

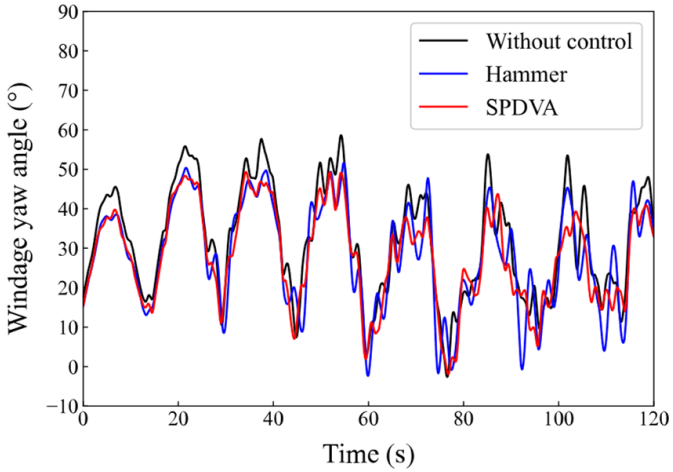

Figure 7. Time history of windage angle response.

Figures 8 and 9 illustrate the displacement and acceleration time history of the insulator's bottom. The peak values of both displacement and acceleration decrease with the use of the heavy hammer and the SPDVA methods compared to the uncontrolled state. In the uncontrolled state, the peak bottom displacement of the insulator is 14.28 m, as illustrated

in Figure 10. When using the heavy hammer, this peak displacement is reduced to 12.59 m, yielding a suppression ratio of 11.83%. With the SPDVA method, the peak displacement is further reduced to 12.22 m, achieving a suppression ratio of 14.43%, which is 2.6% more effective than the heavy hammer.

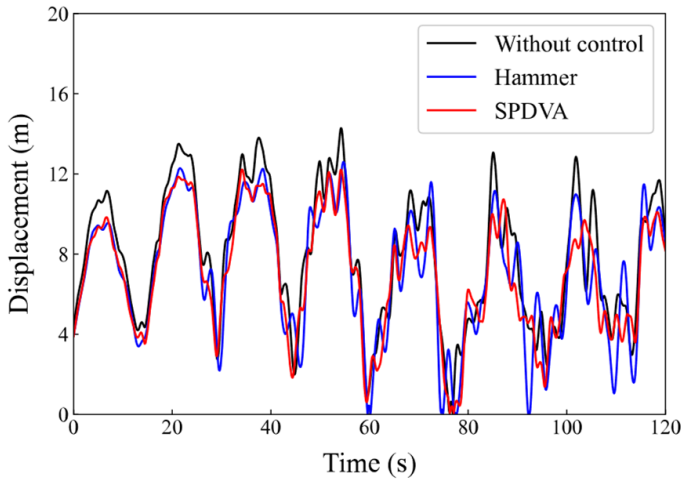

Figure 8. Time history of bottom displacement of insulator.

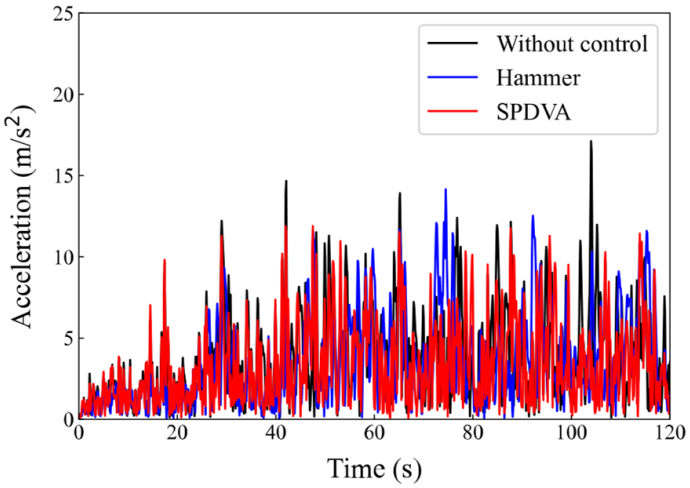

Figure 9. Time history of bottom acceleration of insulator.

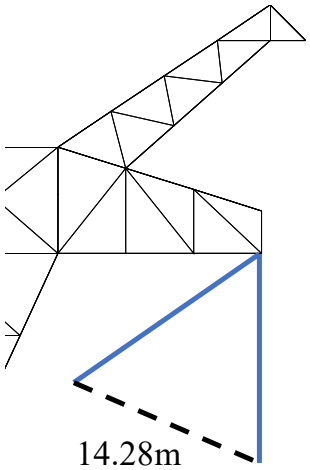

Figure 10. Schematic diagram of peak bottom displacement of the insulator in the uncontrolled state.

Similarly, the peak acceleration at the insulator's bottom is 17.13 m/s^2 in the uncontrolled state. The heavy hammer reduces this peak to 14.16 m/s^2, with a suppression ratio of 17.34%. The SPDVA method reduces the peak acceleration further to 11.90 m/s^2, resulting in a suppression ratio of 30.53%, which is 13.19% more effective than the heavy hammer.

Figure 11 depicts the time history of the insulator's stress response. The peak stress of the insulator increases with the use of the heavy hammer and the SPDVA methods compared to the uncontrolled state. In the uncontrolled state, the peak stress is 108.92 MPa. With the heavy hammer, the peak stress rises to 120.00 MPa, an increase of 11.08 MPa. When using the SPDVA, the peak stress further increases to 123.14 MPa, which is 14.22 MPa higher than the uncontrolled state. Thus, the SPDVA increases the peak stress more than the heavy hammer. This indicates that the additional mass from the heavy hammer and SPDVA installations contributes to a higher insulator stress, which should be accounted for in the design to prevent the tensile fracture of the insulator.

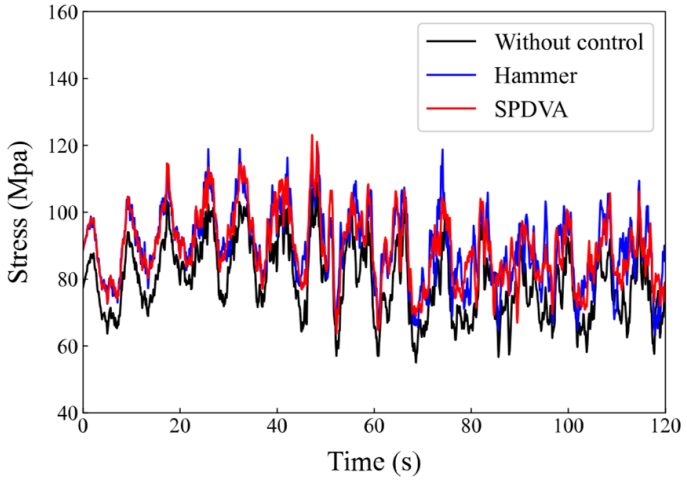

Figure 11. Time history of stress response.

3.3. Impact of Wind Speed

Figure 12 illustrates the impact of wind speed at a 10 m height on the peak windage angle of the insulator. The peak windage angle increases linearly with the wind speed. Both suppression methods reduce the peak windage angle, but the SPDVA consistently achieves a smaller peak angle than the heavy hammer, demonstrating its superior suppression effect.

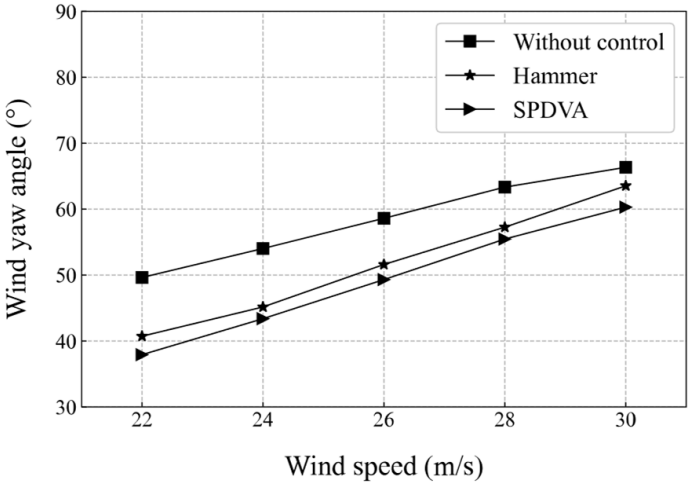

Figure 12. Effect of wind speed on windage angle.

Figure 13 shows the impact of wind speed at 10 m height on the peak displacement and acceleration at the bottom of the insulator. As the wind speed increases, the peak displacement at the bottom of the insulator increases linearly, while the peak acceleration does not change significantly. Both suppression methods reduce the peak displacement, with the SPDVA consistently achieving a smaller displacement than the heavy hammer, indicating better suppression by the SPDVA. Both methods also limit the peak acceleration, but the peak acceleration fluctuates with the wind speed without a clear pattern.

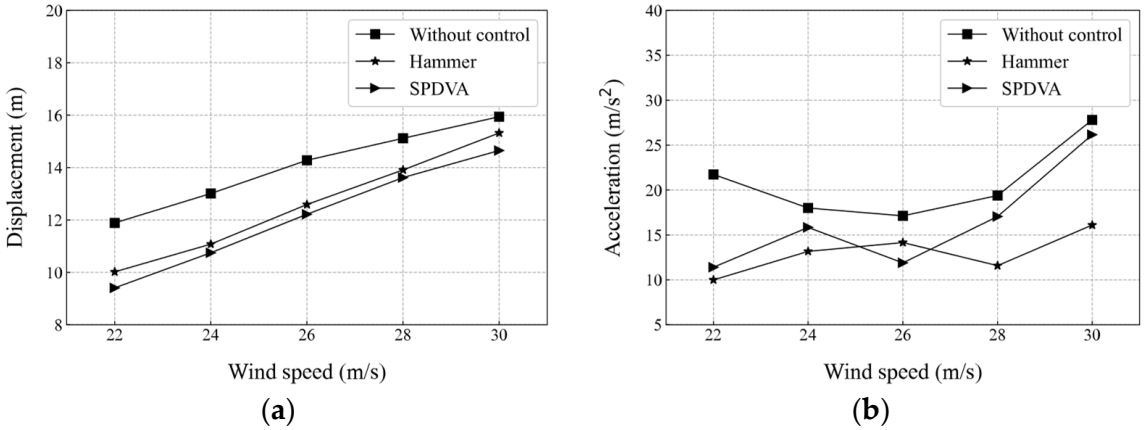

Figure 13. (**a**) Effect of wind speed on displacement of insulator; (**b**) effect of wind speed on acceleration of insulator.

Figure 14 illustrates the influence of wind speed at 10 m height on the peak stress of the insulator. The peak stress increases with the wind speed, and both suppression methods increase the peak stress similarly.

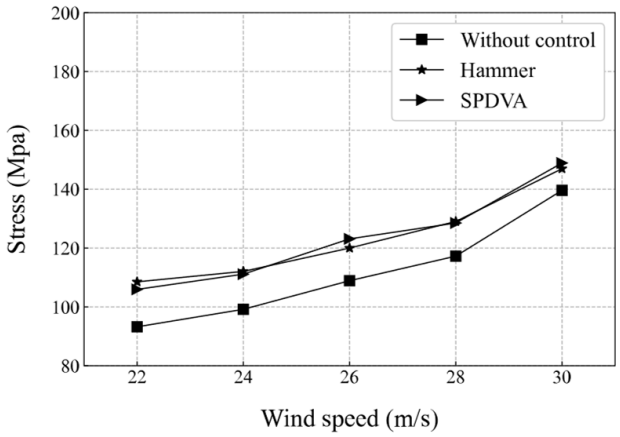

Figure 14. Effect of wind speed on stress response.

3.4. Impact of Spring Stiffness

Figure 15 illustrates the impact of stiffness on the suppression of the windage angle under SPDVA control. As the stiffness increases, the peak and mean square deviation suppression rates initially rise and then fall, with the maximum suppression ratio occurring at 10 kN/m. The peak suppression effectiveness is more pronounced than the mean square deviation suppression effectiveness.

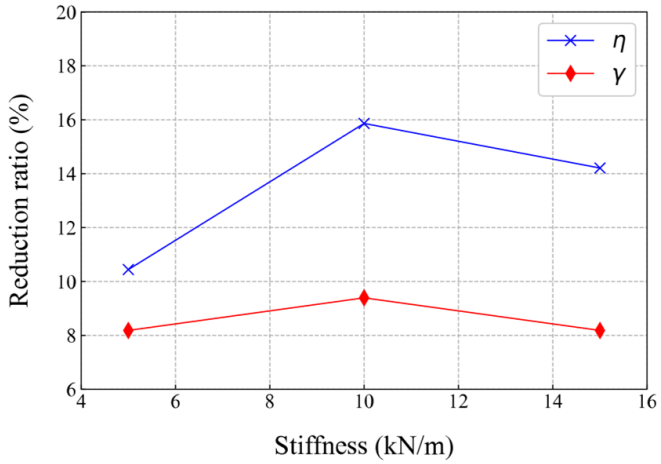

Figure 15. Suppression law of windage angle by SPDVA with different stiffnesses.

3.5. Impact of Mass Block's Mass

Figure 16 illustrates the effect of mass block size on the suppression effectiveness of the windage angle under SPDVA control. As the mass increases, both the peak and mean square deviation suppression ratios improve, with the peak suppression ratio being more effective than the mean square deviation. This indicates that increasing the mass block size can enhance the suppression effectiveness, provided that the insulator's stress limitations are met.

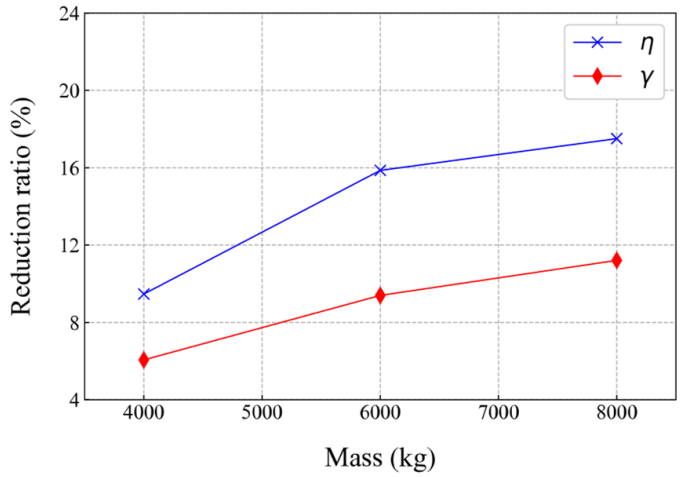

Figure 16. Suppression law of windage angle by SPDVA with different masses.

4. Conclusions

In this study, a spring-pendulum dynamic vibration absorber (SPDVA) is proposed for suppressing the windage response of transmission line systems. A finite element model of a transmission tower-line system is established based on the actual project, and the critical wind speed is determined by analyzing the windage response. The effectiveness of the SPDVA in controlling the windage response of the transmission tower-line system is investigated, and the influence analysis of the mass and stiffness parameters is carried out to further reveal its windage suppression mechanism. The main conclusions are as follows:

(1) As the wind speed increases, the insulator's windage angle rises linearly. Based on the minimum allowable gap between the charged body and the transmission tower structure specified, the maximum allowable windage angle is 58.39°. In this study, a wind speed of 26 m/s at a height of 10 m is identified as the critical wind speed, as it causes the insulator's windage angle to exceed the allowable limit.

(2) As the wind speed increases, the peak windage angle and bottom displacement of the insulator rise linearly, while the peak acceleration at the bottom remains largely unchanged. Compared to the heavy hammer method, the SPDVA provides a more effective suppression, achieving a peak windage angle reduction of up to 15.86%. However, installing the SPDVA also increases the insulator's stress, which must be considered in designing for tensile fracture prevention.

(3) As the stiffness increases, the peak and mean square deviation suppression ratios of the windage angle first increase and then decrease, reaching an optimal stiffness of 10 kN/m. Increasing the mass block's mass also enhances both the peak and mean square deviation suppression ratios of the windage angle. Importantly, the peak suppression effectiveness surpasses the mean square deviation suppression effectiveness across varying parameter changes.

The control effect of the SPDVA proposed in this study on windage response is still to be improved. Combined with the latest research results, the authors' future research will focus on improving the control effect of the existing techniques and developing a new type of measures based on inertial mass amplification technology, so as to provide more effective solutions for the windage response suppression of transmission line systems.

Author Contributions: Investigation, supervision, and writing—original draft, P.S. and X.L.; software, data curation, and writing—review and editing, S.Z. (Sixiang Zhang) and B.Y.; writing—review and editing, S.Z. (Siyao Zhang); conceptualization, resources, supervision, and writing—review and editing, K.R. and L.T. All authors have read and agreed to the published version of the manuscript.

Funding: This research received no external funding.

Data Availability Statement: The datasets generated during and/or analyzed during the current study are available from the corresponding author upon reasonable request.

Conflicts of Interest: Authors Peng Song, Xujun Lang, Sixiang Zhang, Bo Yang were employed by Shandong Electric Power Engineering Consulting Institute Co., Ltd. The remaining authors declare that the research was conducted in the absence of any commercial or financial relationships that could be construed as a potential conflict of interest.

References

1. Li, M.C.; Zhang, Y.L.; Yang, B.G.; Xue, H.; Lv, Y.X.; Zhang, M. Calculation and analysis of suspension insulator strings windage minimum air clearance. *Electr. Meas. Instrum.* **2012**, *49*, 7–10. [CrossRef]
2. Shen, L.; Feng, T.; Liang, S.; Li, C.; Chang, M.; Zhao, Z. Research on the optical fiber monitoring for windage angle of transmission line insulator string. *J. Electr. Power Sci. Technol.* **2021**, *35*, 75–81. [CrossRef]
3. Xu, H.; Zhu, K.J.; Liu, B.; Liu, C.L.; Yang, J.L. A study of influencing parameters on conductor galloping for transmission lines. *J. Vibroeng.* **2014**, *30*, 312–323. [CrossRef]
4. Zhou, L.; Yan, B.; Lu, X.; Liang, M.; Guo, Y.; Yuan, Q. Numerical study on dynamic swing of insulator string in tower-line system under wind load. In Proceedings of the 2012 Asia-Pacific Power and Energy Engineering Conference, Shanghai, China, 27–29 March 2012; pp. 1–4. [CrossRef]
5. Zhao, S.; Yue, J.; Savory, E.; Yan, Z.; Chen, J.; Zhang, B.; Peng, L. Dynamic windage yaw angle and dynamic wind load factor of a suspension insulator string. *Shock. Vib.* **2022**, *2022*, 6822689. [CrossRef]
6. Wang, J.C.; Zhu, S.W.; Peng, B.; Duan, S.B.; Li, P. Static and dynamic mechanical characteristic comparison research of v-type insulator string under gale condition. *IOP Conf. Ser. Earth Environ. Sci.* **2017**, *61*, 012094. [CrossRef]
7. Yin, X.; Shi, Y.; Xu, X.; Duan, Y.; Jia, Y.; Chen, G.; Yin, F. Research on Wind Deviation Detection Based on DENCLUE abnormal Working Condition Filtering. *IOP Conf. Ser. Earth Environ. Sci.* **2020**, *617*, 012015. [CrossRef]
8. Li, L.; Lin, C.; Wu, X. Research on windage yaw of V-type composite insulators in ultra-high voltage. In Proceedings of the Second International Conference on Mechanics, Materials and Structural Engineering (ICMMSE 2017), Beijing, China, 14–16 April 2017; Atlantis Press: Amsterdam, The Netherlands, 2017. [CrossRef]
9. An, L.; Guan, Y.; Zhu, Z.; Zhang, R. Research on windage yaw flashovers of transmission lines under wind and rain conditions. *Energies* **2019**, *12*, 3728. [CrossRef]
10. Liu, Y.; Guo, Y.; Wang, B.; Li, Q.; Gao, Q.; Wan, Y. Research on Influencing Factors and Wind Deflection Warning of Transmission Lines Based on Meteorological Prediction. *Energies* **2024**, *17*, 2612. [CrossRef]
11. Stengel, D.; Mehdianpour, M. Finite element modelling of electrical overhead line cables under turbulent wind load. *J. Struct.* **2014**, *2014*, 421587. [CrossRef]

12. Haddadin, S.; Aboshosha, H.; Ansary, A.E.; Damatty, A.E. Sensitivity of wind induced dynamic response of a transmission line to variations in wind speed. In Proceedings of the Resilient Infrastruct, London, UK, 1–4 June 2016; pp. 1–8.
13. Wang, D.; Chen, X.; Li, J. Prediction of wind-induced buffeting response of overhead conductor: Comparison of linear and nonlinear analysis approaches. *J. Wind. Eng. Ind. Aerodyn.* **2017**, *167*, 23–40. [CrossRef]
14. Li, X.; Zhang, W.; Niu, H.; Wu, Z.Y. Probabilistic capacity assessment of single circuit transmission tower-line system subjected to strong winds. *Eng. Struct.* **2018**, *175*, 517–530. [CrossRef]
15. Mou, Z.; Yan, B.; Lin, X.; Huang, G.; Lv, X. Prediction method for galloping features of transmission lines based on FEM and machine learning. *Cold Reg. Sci. Technol.* **2020**, *173*, 103031. [CrossRef]
16. Fu, X.; Li, H.N.; Li, G.; Dong, Z.Q.; Zhao, M. Failure analysis of a transmission line considering the joint probability distribution of wind speed and rain intensity. *Eng. Struct.* **2021**, *233*, 111913. [CrossRef]
17. Liu, C.N.; Lai, S.K.; Ni, Y.Q.; Chen, L. Dynamic modelling and analysis of a physics-driven strategy for vibration control of railway vehicles. *Veh. Syst. Dyn.* **2024**, 1–31. [CrossRef]
18. Yang, Y.; Liu, C.N.; Chen, L.; Zhang, X.L. Phase deviation of semi-active suspension control and its compensation with inertial suspension. *Acta Mech. Sin.* **2024**, *40*, 523367. [CrossRef]
19. Xu, Z.G.; Wang, T.; Liu, N.B.; Zhang, Z.H.; Dong, S.X. Study on simulation calculation of wind deviation prevention of 220 kV composite insulators. *J. Chongqing Univ. Technol. (Nat. Sci.)* **2023**, *37*, 291–297. [CrossRef]
20. Rao, B.B.; Xu, C.H.; Zeng, X.; Fu, M.H. Analysis and Countermeasures of Wind Deflection Fault of Transmission Line Conductor to Building. *Jiangxi Electr. Power* **2023**, *47*, 1–5. [CrossRef]
21. Chen, M.; Zhang, M. On application of weights to windage suppression for insulator strings on suspension towers. *Guangdong Electr. Power* **2000**, *6*, 18–21. [CrossRef]
22. Zheng, L.Y.; Zhang, J.; Zhu, D.Y. Measures of Preventing Wind Deflection for 500 kV Transmission Lines. *Shandong Electr. Power* **2015**, *42*, 9–13. [CrossRef]
23. Lu, M.; Lin, C.L.; Li, L.; Wang, G.Z. Research on Design of included Angle of UHV V-shape Composite Insulator. *Guangdong Electr. Power* **2018**, *31*, 99–105. [CrossRef]
24. Tian, L.; Zeng, Y.J. Parametric Study of Tuned Mass Dampers for Long Span Transmission Tower-Line System under Wind Loads. *Shock. Vib.* **2016**, *1*, 4965056. [CrossRef]
25. *GB 50665-2011*; Code for Design of 1000kV Overhead Transmission Line. Ministry of Housing and Urban-Rural Development of the People's Republic of China: Beijing, China, 2011.
26. *GB 50009-2012*; Load Code for the Design of Building Structures. Ministry of Housing and Urban-Rural Development of the People's Republic of China: Beijing, China, 2012.
27. Kaimal, J.C.; Wyngaard, J.C.J.; Izumi, Y.; Coté, O.R. Spectral characteristics of surface-layer turbulence. *Q. J. R. Meteorol. Soc.* **1972**, *98*, 563–589. [CrossRef]
28. *IEC 60826-2003*; Design Criteria of Overhead Transmission Lines. International Electrotechnical Commission: Geneva, Switzerland, 2003.